Mg and Mg-Based Blowing Agents for Aluminum Foam

JAYANT BARODE, U. ARAVIND, SANTHOSHKUMAR BHOGI, BISWARANJAN MUDULI, and MANAS MUKHERJEE

In this study, the effectiveness of three different types of Mg-based blowing agents on the structure and properties of aluminum alloy foam was compared. AlMg15Cu10 alloy foams were produced by the powder metallurgy route using pure Mg, Al50Mg50 and Al60Mg40 powders as blowing agents. Al50Mg50 and Al60Mg40 powders were synthesized by ball milling and melt milling, and were characterized by particle size analysis, XRD and SEM. Foams were characterized by using X-ray tomography, SEM and XRD. Mechanical properties were obtained through quasi-static compression tests. It was observed that the foams produced by Mg possess spherical cells whereas more polyhedral cells were obtained in the foams produced by Al50Mg50 and Al60Mg40. The finest cells were produced by Al60Mg40 powder. Variation in the cell size is attributed to the different hydrogen contents of these blowing agents. All foams resulted in a good porous structure and possess high compressive strength compared with conventional foams.

Graphical Abstract

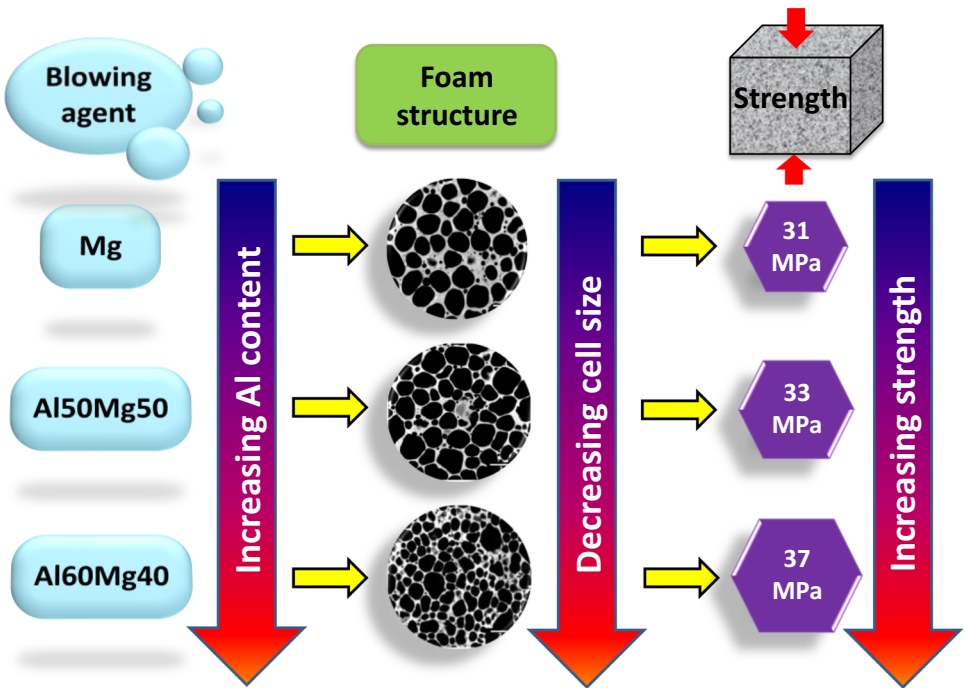

JAYANT BARODE, U. ARAVIND, BISWARANJAN MUDULI, and MANAS MUKHERJEE are with the Department of Metallurgical and Materials Engineering, Indian Institute of Technology Madras, Chennai 600036, India. Contact e-mail: jayant1369@gmail.com SANTHOSHKUMAR BHOGI is with the Department of Basic Science and Humanities, GMR Institute of Technology, Rajam 532127, India

Manuscript submitted June 15, 2020. Accepted October 10, 2020.
Article published online November 6, 2020.

https://doi.org/10.1007/s11663-020-02008-2

I. INTRODUCTION

METAL foam is no longer a new material in science and technology and it is being used in a wide range of applications because of its unique combination of properties.[1] The major applications of metal foam can be classified into structural and functional based on their structure.[1,2] Load-bearing structural application takes advantage of the light weight and specific strength of metal foams [3,4] whereas functional applications are based on their large surface area and interconnectivity.[2,5] The mechanical behavior of foams profoundly depends on their structure,[6] which is indirectly linked to the blowing agent used for foaming.[7]

Blowing agents such as TiH_2 and ZrH_2 are well established for foaming aluminum alloys.[8,9] These hydrides contain a large amount of hydrogen in a concentrated form, which is released over a long span of temperature (or time).[7,10,11] A combination of concentrated gas and its release for a prolonged time is responsible for creating defects as well as large and irregular pores during foaming and solidification.[12,13] Use of Mg-based blowing agents can overcome the challenges of producing defect-free foams. Mg can be hydrogenated by exposing it to a high hydrogen pressure (3 to 47 bar) at high temperatures (300 °C to 450 °C).[14] Mg and Mg-based alloys, however, also contain hydrogen without undergoing any controlled hydrogenation process. They take up hydrogen from the moisture present in the atmosphere even at ambient condition. Jiménez *et al.* found that Al50Mg50 alloy powder contains hydrogen even without undergoing any hydrogenation process.[15] This characteristic was subsequently exploited by Mukherjee *et al.* to foam Al- and Zn-based alloys using Al50Mg50 alloy powder as blowing agent.[16] This blowing agent produced foams with uniform pore size distribution and fine pores containing fewer structural defects compared to the foams produced using conventional blowing agents.

The hydrogen storage capacity of the Mg-based alloys can be altered by varying the Mg content.[14,17] Since the hydrogen content of Al-Mg alloys varies for different sources of Mg, it is of interest to investigate the influence of different sources of Mg on the structure and properties of the foams produced using different Mg-based blowing agents. Therefore, the primary objectives of the present work are (1) to synthesize blowing agents with different Al-Mg ratios, namely Al50Mg50 (wt pct) and Al60Mg40 (wt pct) alloy, and (2) to compare the structure and properties of foams produced using three different sources of Mg-based blowing agents: Mg, Al50Mg50 and Al60Mg40 powders.

II. MATERIALS AND METHODS

A. *Materials*

The elemental metal powders used in the present study were aluminum (Al) (99.5 pct pure, D_{50} = 25 μm), magnesium (Mg) (99.8 pct pure, D_{50} = 119 μm) and copper (Cu) (99 pct pure, D_{50} = 44 μm). All the elemental metal powders were procured from Alfa Aesar. The particle size distribution plots of these powders are shown in the electronic supplementary material (ESM); see Figure S-1. Al (99 pct pure) and Mg (99.9 pct pure) ingots were also used to prepare pre-alloyed powders.

B. *Synthesis of Blowing Agent Powders*

In this study, three blowing agents were used, among which Mg powder was used in as-received condition. Other blowing agents were pre-alloyed powders namely Al50Mg50 (wt pct) and Al60Mg40 (wt pct), which are henceforth referred to as AlMg50 and AlMg40, respectively. Two techniques were employed to synthesize these powders: (1) ball milling (BM) and (2) melt milling (MM). Ball milling was performed on 30 g powder in a tungsten carbide (WC) vial. WC balls (size 10 mm) were used as a grinding media. A ball-to-powder ratio of 10:1 was maintained. Toluene was used as a process-controlling agent. Milling was performed at a rotating speed of 300 RPM for 5 to 20 hours.

In the melt-milling process, first, castings of AlMg50 and AlMg40 alloys were prepared using a bottom pouring furnace under a continuous flow of argon and SF_6 gas mixture. These castings were broken down into small chunks by drilling and then into powdered form by mechanical attrition to obtain finer size. Mechanical attrition was performed under the same conditions as in the ball milling technique. In this, the milling times were 5 minutes, 15 minutes and 1 hour. A 5 g sample was produced per batch.

For the nomenclature of the AlMg50 and AlMg40 blowing agents, the name of the alloy, technique used to prepare the powder and milling time are used in the following form: *alloy-technique used-milling time*.

C. *Precursor Preparation and Foaming*

As-received Mg powder and powders obtained by BM and MM techniques were used as blowing agents to produce foamable precursors of AlMg15Cu10 (all numbers are in wt pct) alloy. The amount of each powder utilized to prepare the precursor using different blowing agents is provided in Table I. Powders were mixed for

Table I. Contribution of Different Powders in AlMg15Cu10 Alloy Precursor

Blowing Agent Used	Amount of Different Powders Used, Wt Pct				
	Al	Cu	Mg	AlMg50	AlMg40
Mg	75	10	15	—	—
AlMg50	60	10	—	30	—
AlMg40	52.5	10	—	—	37.5

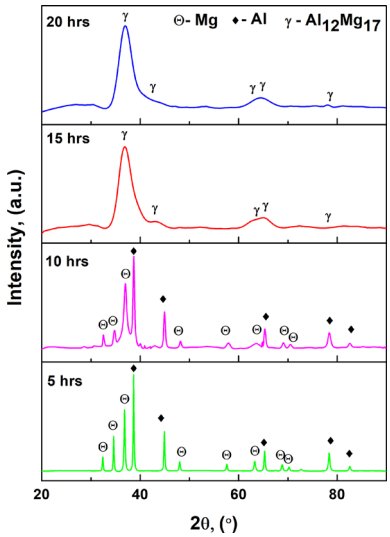

Fig. 1—XRD patterns of AlMg50 powders ball milled for 5, 10, 15 and 20 h.

15 minutes in a custom-made mixer. Ten grams of powder blend was consolidated by hot uni-axial compaction at 450 °C for 20 minutes applying a pressure of 500 MPa. This resulted in cylindrical precursors of 36 mm diameter with 4 mm thickness. The precursor was cut into four equal pieces, and each piece was foamed using a ceramic heating plate. Foaming was performed by heating the precursor to 600 °C for 2 minutes. Subsequently, the heating was switched off followed by cooling of the sample by directing pressurized air. Air pressure was adjusted to prevent any damage to the foam.

Phase analysis of the blowing agents and foam was carried out by an X-ray diffractometer (X'pert Pro PANalytical) using monochromatic Cu-Kα radiation of 1.54 Å wavelength with a step size of 0.02 deg. Powder morphology and foam microstructure were observed using a scanning electron microscope (FEI SEM Quanta 200). Particle size of the powders was measured by Microtrac S3500. Hydrogen content of the blowing agent was determined by a Thermo Scientific Flash 2000 Organic Elemental Analyzer performed in CHNS/O mode.

The porous structure of foams was observed by X-ray computed tomography using a laboratory-based source equipped with a 240 kV/320 W micro focus X-ray tube and a flat panel detector. VG Studio-Max 2.1 software was used to extract 2D sections from the tomographic data. The 2D sections (20 sections per foam) were analyzed using ImageJ 1.42q software. Compression test was performed using a universal testing machine (UTM) at a displacement rate of 1 mm/min. The average foam sample size for compression tests was $10 \times 10 \times 8$ mm^3, and the least dimension, which was also the foaming direction, was considered as the compression direction.

III. RESULTS

A. *Blowing Agents*

1. *Phase Analysis*

The XRD spectrum of AlMg50-BM-5-20 hours is shown in Figure 1. Individual peaks of Al and Mg can be seen even after 5 and 10 hours of milling. Broadening of peaks is observed after 15 hours, and some peaks become much clearer after 20 hours. De-convolution of the peaks (in 20 hours sample) confirmed the overlap of (1) 41.94 and 43.74 deg; (2) 62.20 and 64.93 deg; (3) 76.61 and 77.87 deg (2θ) peaks. This pattern corresponds to the γ-$Al_{12}Mg_{17}$ phase.

Powder processed by the MM route revealed the formation of intermetallic phases, γ-$Al_{12}Mg_{17}$ and β-Al_3Mg_2, for the alloy composition of AlMg50 and AlMg40, respectively; see Figure 2. Mg_2Si was also present as a minor phase in AlMg50 powder.

2. *Powder Size and Morphology*

SEM micrographs of the as-received Al, Mg and Cu powders are shown in Figure 3. Powders processed by the BM and MM route are shown in Figure 4. AlMg50-BM-20 hours and AlMg50-MM-1 hours reveal a flaky morphology, whereas AlMg50-MM-15 minutes and AlMg40-MM-5 minutes powders do not show flaky or platelet morphology but possess faceted cleavage as shown in Figure 4(b). No flaky structures are observed in as-received Al, Mg and Cu powders.

3. *Hydrogen Content and Surface Area*

Hydrogen content of the materials (except Cu powder) is presented in Table II. Hydrogen content of the blowing agents was normalized with respect to the BET surface area, which is also provided in Table II along with the surface area normalized hydrogen contents. It can be seen that Al powder and the ingots used in this study have almost no hydrogen, whereas all the blowing agents (both the as received and custom made) have a significant amount of hydrogen.

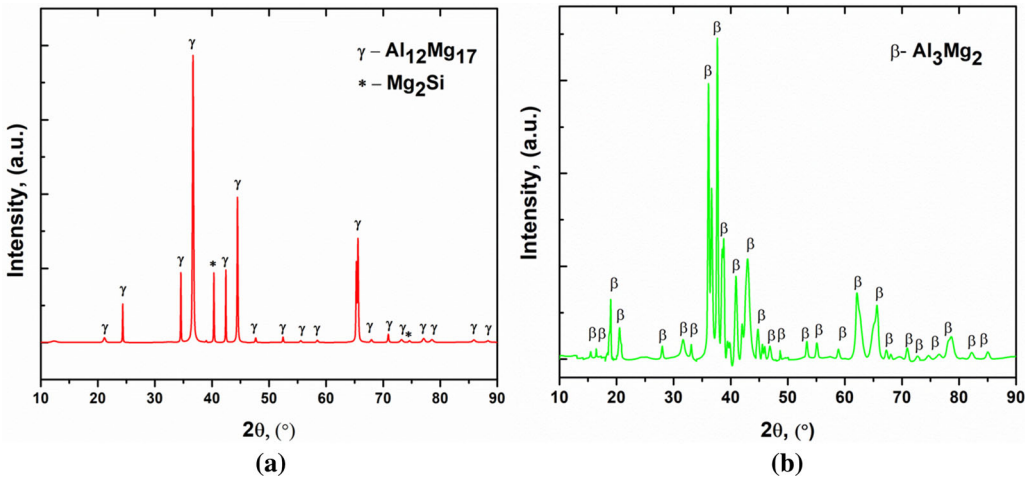

Fig. 2—XRD pattern of (*a*) AlMg50-MM-15 min and (*b*) AlMg40-MM-5 min powder.

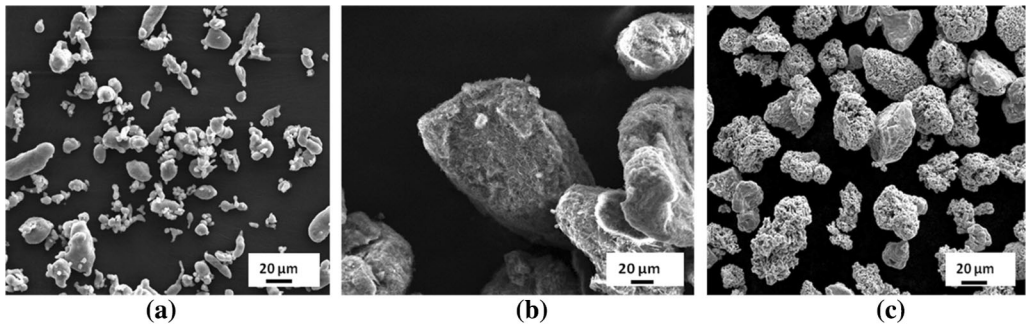

Fig. 3—SEM images of as-received powders: (*a*) aluminum, (*b*) magnesium and (*c*) copper.

B. *Foams*

1. *Foam Structure*

Photographs of the foams produced by using various blowing agents are shown in Figure 5. Foams produced by using AlMg50-BM-20 hours and AlMg50-MM-1 hours powders did not yield a satisfactory porous structure (Figures 5(a) and (b)), whereas Mg, AlMg50-MM-15 minutes and AlMg40-MM-5 minutes powders resulted in a good porous structure (Figures 5(c) through (e)).

Hereafter, all the analysis presented is from the three types of foams that exhibited a good porous structure as shown in Figures 5(c) through (e). The relative density and expansion (calculated based on relative density) are listed in Table III. It can be seen that foams produced by using AlMg40-MM-5 minutes have the highest expansion. The 2D tomographic sections of the foams and their corresponding cell size distributions are shown in Figure 6. The average D_{mean} values are provided in Table III. Foams produced by using AlMg40-MM-5 minutes have the smallest cell size.

Morphology of the porous structure of the foams was analyzed in terms of their circularity in Figure 7. Circularity (C) of a cell is defined as a degree to which a cell is similar to the circle having a diameter equal to its equivalent diameter, taking into consideration the smoothness of the perimeter, *i.e.*, as the shape becomes rounder and smoother, the circularity approaches 1. Circularity is calculated using the following equation.

$$C = 4\pi \frac{\text{Area}}{\text{Perimeter}^2} \quad [1]$$

Foam produced using Mg has a mean circularity of 0.97, indicating that cells are mostly spherical, octagonal or near hexagonal shape. AlMg50-MM-15 minutes and AlMg40-MM-5 minutes powders resulted in cells of polyhedral shape (hexagonal or pentagonal shape), both having mean circularity of 0.86.

2. *Microstructure and Phase Analysis*

SEM micrographs of the foams are shown in Figure 8. Uniform distribution of bright phase embedded in a dark matrix can be observed in all the microstructures. Foams were crushed into powders to determine the phases present in the microstructure. The XRD spectrum of the powdered-foam samples presented in Figure 9 reveals that foams consist primarily of two phases: Al and Al_2CuMg. A comparison of their relative amount suggests that the Al phase and Al_2CuMg phase correspond respectively to the dark matrix and bright phase in the cell wall microstructure.

3. *Stress–Strain Behavior*

Compression behavior of the foams was determined by testing three samples from each blowing agent category. Typical stress–strain curves of these foams are presented in Figure 10, and the results are summarized in Table III. H/D_{mean} values of all the samples tested were > 5, where H is the smallest dimension of the sample used for the compression test. $H/D_{mean} > 5$ is required to avoid the size effect on the compressive strength of foams.[18,19] Compressive strength (σ_p) of foam is the first peak after the elastic region of the stress–strain curve. Densification strain (ε_d) is the strain at which the densification of the foam begins, which is indicated by a sudden rise in the stress without a significant change in the strain. A similar trend in the stress-strain curve was seen in all three foams: a sudden dip in stress immediately after reaching the compressive strength, which is followed by a number of serrations (jerky flow) in the plateau region till the densification strain is reached.

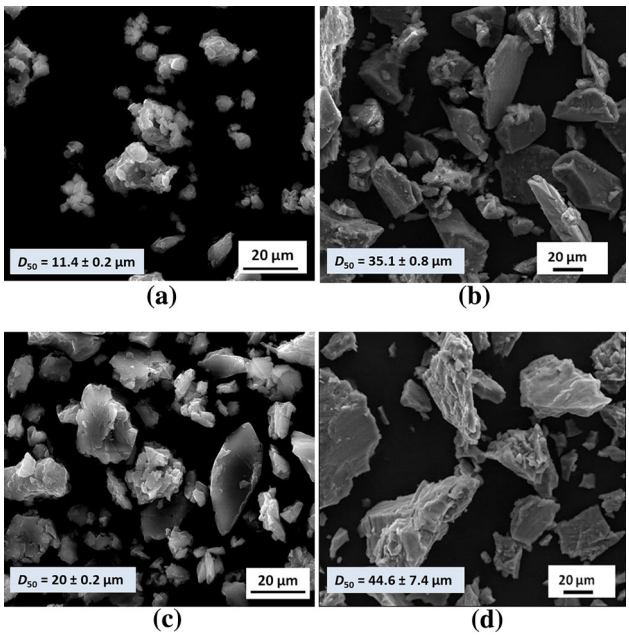

Fig. 4—SEM micrographs and particle size of (*a*) AlMg50-BM-20 h, (*b*) AlMg50-MM-15 min, (*c*) AlMg50-MM-1 h and (*d*) AlMg40-MM-5 min. Here, D_{50} values are an average of eight measurements, and the error bar represents the standard deviation. (For particle size distributions of all the powders refer to Fig. S-1 in the ESM).

IV. DISCUSSION

A. *Selection of Blowing Agent*

Each blowing agent chosen for this study consists of a single phase. Mg, AlMg50 and AlMg40 consist of pure Mg, γ-$Al_{12}Mg_{17}$ and β-Al_3Mg_2, respectively. This automatically ensures a uniform distribution of Mg throughout each blowing agent powder particle. In this way, the choice of the blowing agents offered three different sources of Mg, which not only contain different amounts of hydrogen (see Table II) but also were expected to have different hydrogen desorption behaviors during foaming.[14] Because of this, we could study the effect of different sources of Mg on the foaming behavior and resultant foam properties. Any other composition in the Al-Mg system would mean a mixture of two of the aforementioned phases,[20] and consequently the blowing agent would become a mixture of two different types of blowing agents.

B. *Foamability of a Precursor*

The foamability of the precursors depends on the degree of compaction. Here, the 'degree of compaction' refers to a combination of the 'degree of mechanical interlocking' and 'degree of metallic bonding.' During compaction, powder particles are pressed against each other, leading to an interparticle movement, breaking of the oxide layer and mechanical interlocking. This improves the packing density of the compact. During sintering, these mechanically interlocked particles develop metallic bonding by diffusion of atoms, which further improves the density of the compact. Thus, both the degree of mechanical interlocking and degree of metallic bonding are responsible for the degree of compaction. Mechanical interlocking is a pre-requisite for developing metallic bonding during sintering and is significantly influenced by the particle size and morphology. AlMg50-BM-20 hours powder particles having

Table II. Hydrogen Content of the Ingots and Various Powders Along with Their Surface Area and Surface Area Normalized Hydrogen Content of the Blowing Agents. The Definition of 'Estimated Hydrogen Content' is Provided in Section IV–C

Material	Hydrogen Content, Wt Pct	BET Surface Area (m^2/g)	Surface Area Normalized Hydrogen Content, g/m^2	Estimated Hydrogen Content Based on Mg Content, g/m^2
Al powder	0	not measured	—	—
Mg powder	0.64 ± 0.03	1.89	0.0033	0.0033
Al ingot	0.04 ± 0.04	not measured	—	—
Mg ingot	0.01 ± 0.01	not measured	—	—
AlMg50-BM-20 h powder	1.3 ± 0.03	not measured	—	—
AlMg50-MM-15 min powder	0.50 ± 0.03	1.89	0.0026	0.0016
AlMg40-MM-5 min powder	0.46 ± 0.01	2.45	0.0018	0.0013

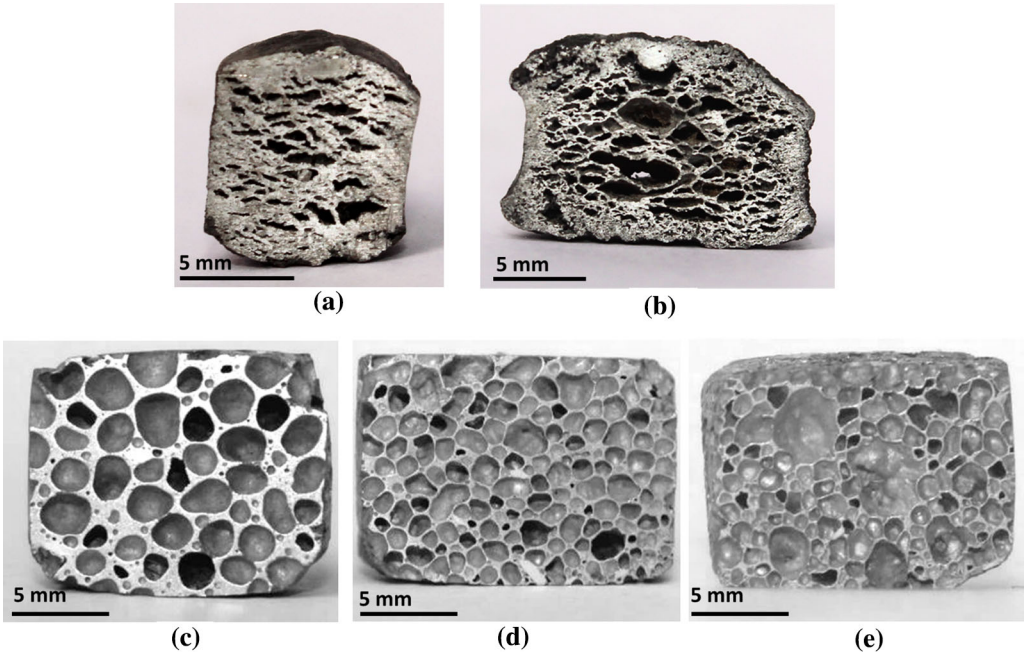

Fig. 5—Sections of foams along the foaming direction produced by using (*a*) AlMg50-BM-20 h, (*b*) AlMg50-MM-1 h, (*c*) Mg, (*d*) AlMg50-MM-15 min and (*e*) AlMg40-MM-5 min powders.

D_{50} = 11 μm are much finer than those with AlMg50-MM-15 minutes (D_{50} = 35 μm) and AlMg50-MM-1 hour (D_{50} = 20 μm); see Figure 4. In addition to the fine particle size of AlMg50-BM-20 hours, they are also brittle in nature. AlMg50 powders consist of a brittle intermetallic phase (γ-$Al_{12}Mg_{17}$) [21] as shown in Figures 1 and 2(a). It is known that brittle particles of small size are much more difficult to consolidate.[22] The combination of fine size and brittle nature could be one of the reasons for the mismatch between the AlMg50-BM-20 hours (blowing agent) and the other metal powder (Al and Cu) during hot compaction, leading to a poor consolidation of the precursor. Another parameter that affects the compatibility of the powders is the shape of the powder particle. AlMg50-BM-20 hours powders revealed a flaky morphology; see Figure 4(a). This is because ball milling usually produces powders of flaky or platelet morphology.[23] In the initial stages of milling, Al (ductile) powder particles get flattened by the ball-powder collision, while Mg (brittle) particles get fragmented and eventually embedded in the flat Al particles. This results in a flaky morphology. On the other hand, AlMg50-MM-15 minutes powder exhibited faceted cleavages, as shown in Figure 4(b). In the MM route, pre-alloying through melting produced the desired intermetallic phase. Therefore, the subsequent milling of the brittle phase did not result in a flaky morphology. However, when the milling time is increased to 1 hour, the same powder converts into a flaky morphology as was observed in the case of AlMg50-MM-1 hour powder; see Figure 4(c). Flaky or platelet morphology reduces the packing density of the powder compact, which results in a higher degree of porosity in the sintered materials.[24,25] Encapsulation of the blowing agent during compaction is a necessary condition in the production of metal foam.[26,27] Otherwise, the evolved gas would escape through the cracks formed in between the blowing agent particles and metallic matrix. As-received powder particles of Al, Mg and Cu do not have any flaky and platelet characteristics; see Figure 3. AlMg40 ball-milled powders were also produced, but the BM technique did not result in the desired β-Al_3Mg_2 phase even after 60 hours of milling. The XRD spectrum for the milling time of 20 to 60 hours is shown in the ESM (Figure S-2). Since AlMg40 ball-milled powders exhibited a similar flaky morphology as AlMg50-MM-20 hours powder, they were not used for foaming. SEM image of AlMg40-BM-20 hours is shown in the ESM (Figure S-3).

Although there is not much difference in the particle size of AlMg50-MM-15 minutes and AlMg50-MM-1 hour powders, there is a significant change in the particle morphology (faceted to flaky); see Figures 4(b) and (c). Flaky or platelet morphology is a characteristic of ductile powders although the XRD pattern of AlMg50-MM powder indicates that it mainly consists of the intermetallic brittle γ-$Al_{12}Mg_{17}$ phase (Figure 2(a)). This brittle-to-ductile transition of the AlMg50-MM powders during milling is atributed to their small crystallite size. To get an approximation of the crystallite size (τ) of this powder, the Scherrer equation was used.

$$\tau = \frac{K\lambda}{\beta \cos\theta} \qquad [2]$$

here θ is the Bragg angle and β is the line broadening at half the maximum intensity (FWHM), λ is the wavelength of the X-ray (1.54 Å), instrument

Table III. Relative Density, Expansion, D_{mean} and Compressive Strength of the Foams Prepared Using Different Blowing Agents. All the Values Presented Are an Average of Three Foams from Each Category

Blowing Agent Used	Relative Density of Foam, ρ^*	Average Expansion, Pct	Average D_{mean}, mm	Average Compressive Strength, σ_p (MPa), Pct	Highest Compressive Strength in Each Category, σ_p (MPa)
Mg	0.27 ± 0.01	267 ± 11	1.17 ± 0.11	26.7 ± 13	31.0
AlMg50-MM-15 min	0.31 ± 0.05	229 ± 46	0.98 ± 0.06	28.7 ± 15	33.3
AlMg40-MM-5 min	0.26 ± 0.02	275 ± 17	0.68 ± 0.02	24.4 ± 46	37.3

broadening = 0.001 (2θ), and the shape factor K = 0.9. AlMg50-MM-1 hour powder has a lower crystallite size (τ = 27 nm) than AlMg50-MM-15 minutes powders (τ = 36.5 nm). It was reported that ceramics as well as intemetallics show a sudden increase in strain rate sensitivity when the grain size becomes finer because of a combination of several factors such as grain boundary sliding, the presence of defects and rapid short range diffusion.[28,29] During the milling process, powder particles undergo repeated cold working by the impact of hard WC balls causing a significant reduction in their crystallite size. This causes the transition from brittle to ductile nature and consequently a change in the morphology of the powder particles. This is responsible for the poor consolidation of the powder resulting in poor foamability of the precursor.

Foamability of the precursors prepared with AlMg50-BM-20 hours and AlMg50-MM-1 hour powders was also investigated by varying all the compaction parameters: pressure, temperature and time. However, none of them resulted in a satisfactory foam structure. Results of these trials are provided in the ESM, Tables S-I and S-II. Note that AlMg50-BM-20 hours powders contains the highest amount of hydrogen (see Table II). Therefore, unsucessful foaming is not because of a lack of hydrogen in this powder.

Precursors prepared with Mg as a blowing agent resulted in a good foam structure as shown in Figure 5(c). This is because Mg does not have a flaky morphology. Also, the presence of Mg improves the sintering behavior of Al powders by rupturing the thick Al_2O_3 surface layer, which acts as a barrier during sintering, thereby facilitating diffusion and wetting of the primary powder particles.[30,31]

C. *Influence of the Source of Mg on the Foam Structure*

Foam produced by using AlMg40-MM-5 minutes powder contains finer cells (D_{mean} = 0.68 mm) than those produced by using AlMg50-MM-15 minutes (D_{mean} = 0.98 mm) and Mg (D_{mean} = 1.17 mm) powders. The difference in cell size obtained using different blowing agents is attributed to the different sources of Mg, which determine the amount of gas present in the powders. As the particle sizes of these blowing agents are not similar, it is difficult to compare the gas content of the powders since the higher the surface area is, the higher the gas absorption capability. Therefore, to compare the gas content of the blowing agents, the hydrogen content of each blowing agent has been normalized by their respective BET surface area. It was found that AlMg40-MM-5 minutes powder has the lowest hydrogen content among the three blowing agents (see Table II). This is because hydrogen reacts only with Mg, and Al does not take up hydrogen under ambient conditions.[32] Increasing the Al content reduces the weight fraction of Mg in the alloy and consequently reduces the hydrogen absorption of the alloy powder.[17] Therefore, AlMg40-MM-5 minutes powder produces small bubbles, which lead to finer cells. A physical model by Körner *et al.* [33] considered micro crack and pores as nucleation sites for bubble nucleation, which seems to be a valid assumption in the case of the precursors prepared by powder metallurgical route. Hydrogen released from the blowing agents diffuses to these nucleation sites causing them to inflate. The gas pressure inside the bubble, which is responsible for its growth, is related to the dissolved hydrogen concentration at the gas-melt interface according to Sieverts' law. The growth of the bubble is thus restricted by the dissolved gas in the melt, which in turn is directly controlled by the gas content of the blowing agent. Therefore, the presence of finer cells is a consequence of a lower gas content of the blowing agent.

Although AlMg40-MM-5 minutes powder has the lowest hydrogen content, it still contains hydrogen slightly higher than it is supposed to have if hydrogen is stored only in the Mg present in this alloy powder. The surface area normalized value of Mg is 0.0033 g/m^2. Therefore, by considering the respective Mg content in AlMg50-MM-15 minutes and AlMg40-MM-5 minutes powders, the hydrogen content in these two powders should be 0.0016 and 0.0013 g/m^2, respectively. These values are referred to as the 'estimated hydrogen content' in Table II. However, the actual hydrogen content of these powders is higher: 0.0026 and 0.0018 g/m^2, respectively. This slightly higher hydrogen content of these powders could be due to the presence of Al and a different hydrogen uptake behavior of the intermetallic

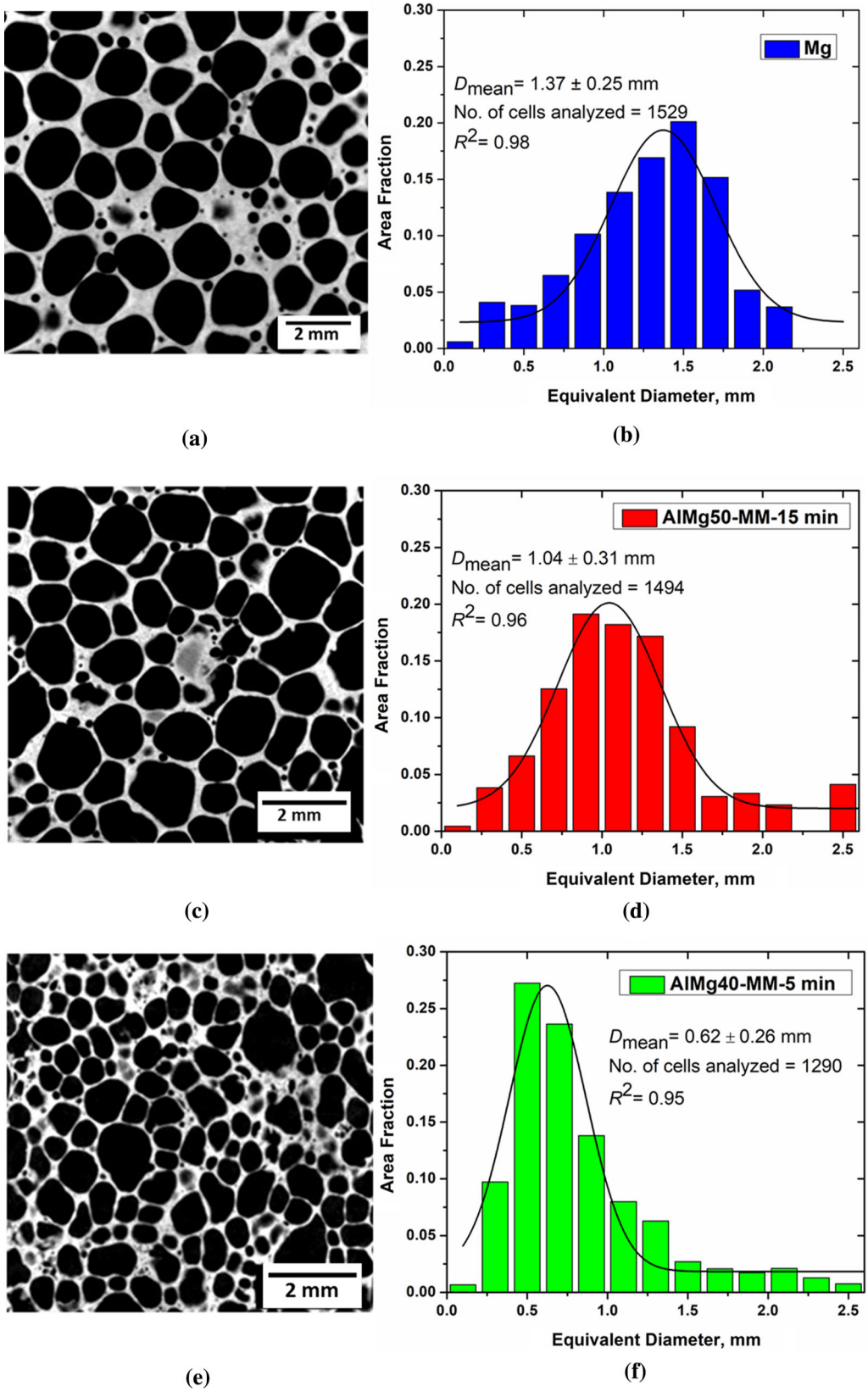

Fig. 6—Representative 2D X-ray tomograms and their corresponding cell size distribution of the AlMg15Cu10 foams prepared using three different blowing agents: (*a*, *b*) Mg, (*c*, *d*) AlMg50-MM-15 min and (*e*, *f*) AlMg40-MM-5 min powders. (Cell size distributions were fitted using a Gaussian function. R^2 represents goodness of the fit.).

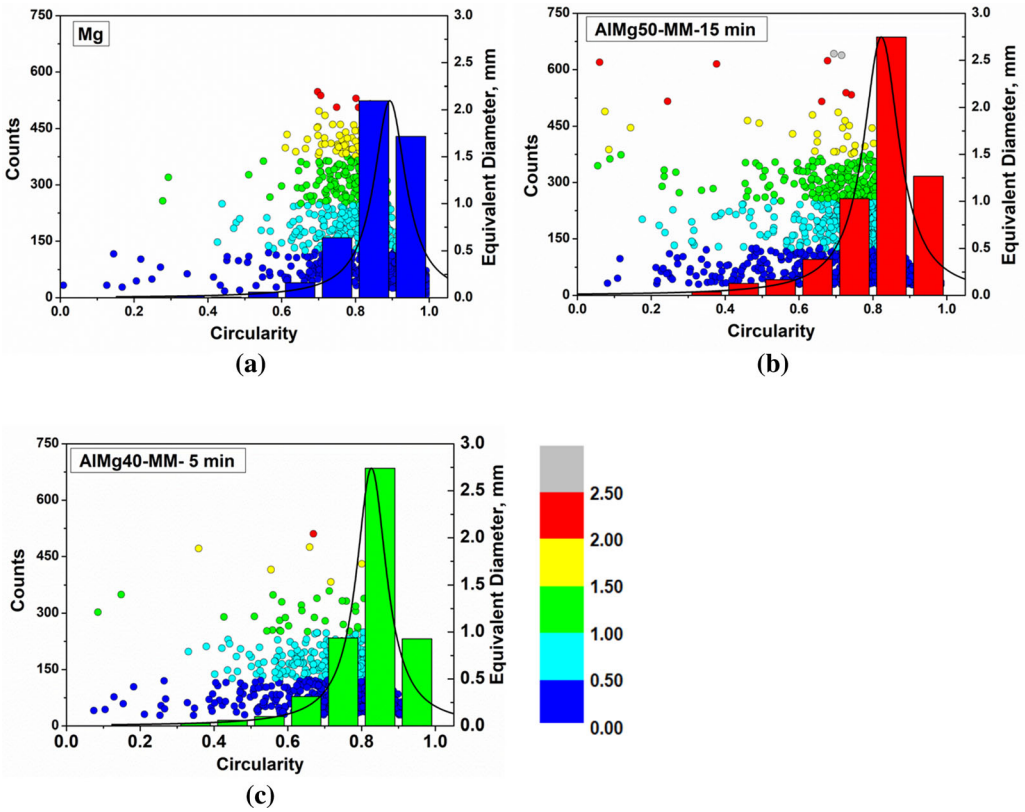

Fig. 7—Circularity *vs.* counts (bars) and circularity *vs.* equivalent diameter (circles) of foams prepared using (*a*) Mg, (*b*) AlMg50-MM-15 min and (*c*) AlMg40-MM-5 min powders. Circularity *vs.* counts plot was fitted with a Lorentz function (solid line) to determine mean circularity. (Color scale is for equivalent diameter of cells.).

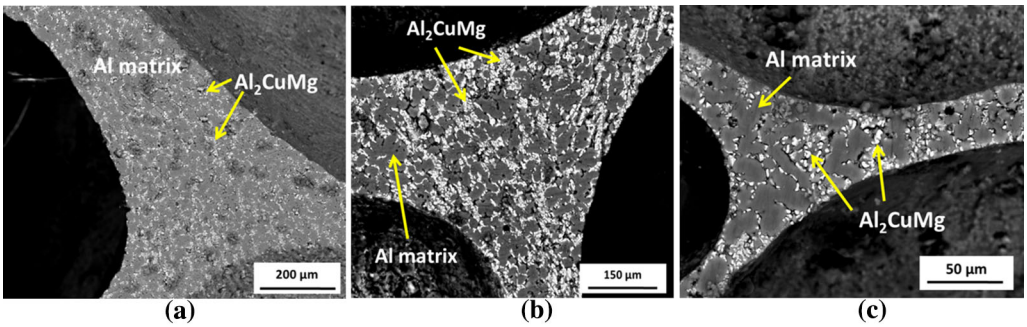

Fig. 8—SEM (BSE mode) micrographs of cell walls in foams produced using (*a*) Mg, (*b*) AlMg50-MM-15 min and (*c*) AlMg40-MM-5 min blowing agents.

phases compared to that of pure Mg. It has been reported that the presence of Al facilitates hydrogen diffusion, which usually gets blocked because of the formation of a stable magnesium hydride film.[34] The surface of Mg particles is usually contaminated because of the formation of MgO or $Mg(OH)_2$.[35,36] On the other hand, intermetallic γ-$Al_{12}Mg_{17}$ and β-Al_3Mg_2 phases are less prone to oxygen contamination. Hydride-forming intermetallic compounds are known to react with hydrogen even at room temperature.[37,38]

The circularity values of the three types of foams are not similar; see Figure 7. The variation in the porous structure of the foams produced using different blowing agents is arising because of a difference in the number of gas nucleation sites present in the precursor. In addition to the typical nucleation sites in the powder metallurgical precursor, blowing agents can also act as gas nucleation sites. All the three blowing agents consist of brittle phase, which makes it difficult to completely bond with the Al matrix during compaction. As a result, the interfaces between the Al matrix and blowing agent particles may act as gas nucleation sites.[39,40] The number of blowing agent-based nucleation sites present in the precursor were estimated. For this, particles were assumed to be spherical with a diameter equivalent to their D_{mean}, and each blowing agent particle is considered to correspond to at least one nucleation site. The minimum number of nucleation sites or the particles for

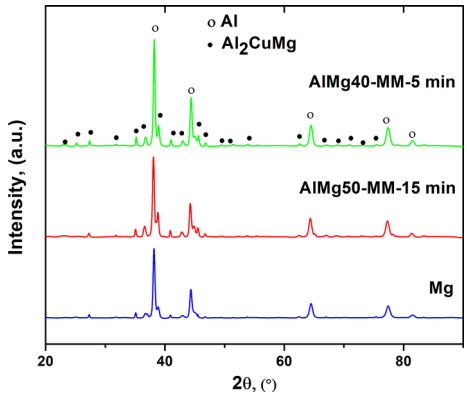

Fig. 9—XRD patterns of the powdered AlMg15Cu10 alloy foams produced using Mg, AlMg50-MM-15 min and AlMg40-MM-5 min powders as blowing agent.

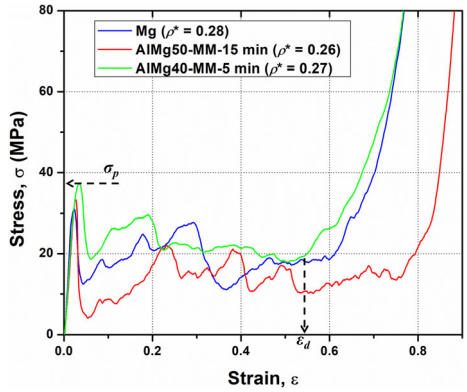

Fig. 10—Stress-strain curves of three representative foams prepared using Mg, AlMg50-MM-15 min and AlMg40-MM-5 min powders.

each blowing agent are displayed in Table IV. Mg powders, being large and contributing only 15 pct of the total weight of the precursor, contribute a smaller number of nucleation sites compared to other blowing agents. As a result, in the case of Mg blowing agents, the bubbles are mostly spherical because of a lack of interactions with the neighbors. Bubbles remain spherical until they touch each other or, to be precise, deformed by neighboring bubbles. On the other hand, when 30 wt pct AlMg50-MM-15 minutes and 37.5 wt pct AlMg40-MM-5 minutes powders are used, the precursors contain two orders of magnitude higher nucleation sites compared to Mg-based precursors. A large number of gas nucleation sites can generate a large number of bubbles, causing more bubble-bubble interactions. Princen *et al.* reported that when bubble-bubble interaction increases, the bubbles are no longer spherical but are deformed into a more or less polyhedral structures.[41]

D. *Effect of Micro- and Macrostructure on the Compressive Properties*

Compressive properties of a foam are influenced by its relative density, microstructure, macro- and macrostructural defects.[4,42] The presence of serrations in the plateau region in Figure 10 indicates that foams are brittle in nature. This is because of the presence of a large amount of intermetallic phase (Al_2CuMg) in the microstructure, as revealed in Figures 8 and 9. The formation of this intermetallic phase during solidification is also responsible for a high compressive strength of the foams compared to conventional aluminum foams.[4,16]

In the present study, the effect of microstructure on compressive strength can be ignored as all types of foams possess similar microstructure and phases (Figures 8 and 9). Therefore, the variation in the compressive strength of foams can be attributed to their relative density and macrostructural effects. It can be observed that there is a considerable deviation in the compressive strength of all the foams, especially in the case of AlMg40-MM-5 minutes powders as implied by a high standard deviation ($\approx$ 45 pct); see Table III. This high standard deviation is due to the presence of a relatively large number of structural defects in these foams as demonstrated in the following. Defect analysis was performed by examining the 2D X-ray tomograms of all the foams. A total of nine foams (3 from each blowing agent category) and ten 2D tomograms containing approximately 2000 cells of each foam were analyzed. The analysis in terms of the area fraction of large cells is presented in Table V. Large cells are defined by the following criteria: $D_{\text{large-cell}} > 2D_{\text{mean}}$, as suggested by Mukherjee *et al.*[6] The area fraction of large cells is considered as a measure of defects because large cells are considered to be weak links as deformation generally initiates at larger cells.[43,44] Foams produced using AlMg40-MM-5 minutes contain 16 pct area fraction of large cells, whereas those produced using Mg and AlMg50-MM-15 minutes contain only 6 pct and 8 pct, respectively. One of the 2D tomograms of the defect-rich zone in AlMg40-MM-5 minutes blowing agent-based foam is shown in Figure 11.

E. *Influence of Cell Size on Compressive Strength*

Large cells cause high standard deviation in the compressive strength of foams as explained above. Therefore, to compare the foams prepared using different blowing agents, foam with the least area fraction of large cells in each category is considered. The stress-strain behavior of these foams is presented in Figure 10. Relative densities of these foams are similar, and thus the density-normalized compressive strength follows the same trend as the compressive strength. Foam produced with AlMg40-MM-5 minutes powder shows the highest

Table IV. Amount and Number of Blowing Agent Particles Present in the Foamable Precursor Prepared with Different Blowing Agents

Blowing Agent	Amount Used in the Precursor, Wt Pct	Number of Particles in a 10 g Precursor, $\times 10^5$
Mg	15	9.6
AlMg50-MM-15 min	30	610
AlMg40-MM-5 min	37.5	409

Table V. Area Fraction of Large Cells for Foams Produced Using Various Blowing Agents

Blowing Agent	Area Fraction of Large Cells $D_{\text{large-cell}} > 2D_{\text{mean}}$ (Pct)
Mg	6 ± 5
AlMg50-MM-15 min	8 ± 3
AlMg40-MM-5 min	16 ± 6

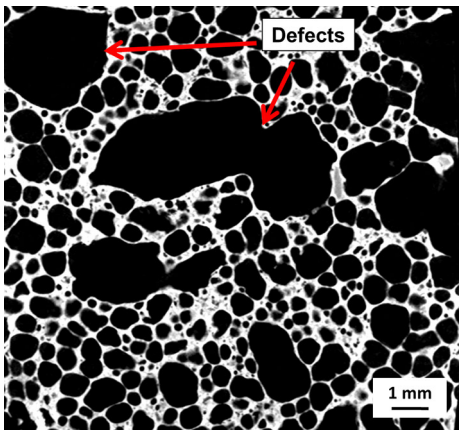

Fig. 11—The 2D X-ray tomogram showing defects in foam produced by using AlMg40-MM-5 min powder.

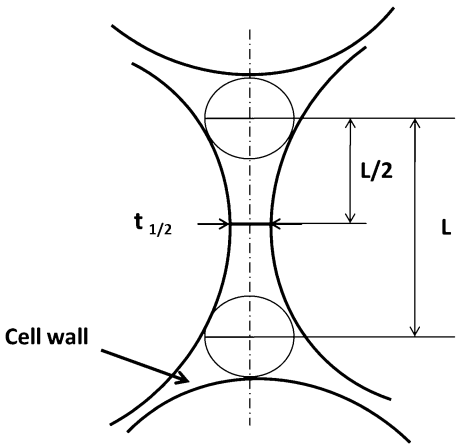

Fig. 12—Schematic illustration of a cell wall showing the structural parameters.

compressive strength of 37.3 MPa. This variation can be explained in terms of cell morphology. A similar approach was considered for analyzing cell walls as described by Miyoshi *et al.*[45] The schematic of a cell wall is shown in Figure 12. The apparent cell edge length is L. Cell wall thickness $t_{1/2}$ was measured at $L/2$. From 2D X-ray tomograms, approximately 100 cells per foam were analyzed to extract these structural parameters. The data are presented in Table VI.

The average L decreases with decreasing cell size. Since AlMg40-MM-5 minutes powder produces the smallest cells, this foam has the shortest L. This results in a high aspect ratio ($t_{1/2}/L$). An increase in the aspect ratio of the cell wall increases the bending strength by offering a greater resistance against buckling. It is known that metal foam fails by buckling of the cell walls,[6,46,47] and therefore a higher aspect ratio in the case of foam produced using AlMg40-MM-5 minutes enhances the overall strength of these foams. Wen *et al.* reported that the peak stress of Mg foam increases from 11 to 16 MPa when the average pore size decreases from 412 to 73 μm.[48] Miyoshi *et al.* found that with the reduction in mean pore size from 4.5 mm to 3 mm the compressive strength of Al foams increases by 40 pct.[45] Thus, the foam produced by using Mg has the lowest strength due to their smallest aspect ratio.

V. CONCLUSION AND OUTLOOK

Ball-milling and melt-milling techniques were employed to synthesize Al-Mg blowing agent powders. The melt-milling technique produced both γ-$Al_{12}Mg_{17}$ and β-Al_3Mg_2 phases, whereas the ball-milling technique produced only γ-$Al_{12}Mg_{17}$ phase. The hydrogen content of the blowing agents decreases with a reduction in Mg content. Pure Mg powder and the powders prepared by the melt-milling technique were successful in producing foams with good structures and uniform cell size distribution, whereas the powders prepared by ball milling did not result in a satisfactory foam structure because of their flaky or platelet-like particle morphology.

Among the three blowing agents, AlMg40 powders produced the smallest cells because of their lowest hydrogen content. Cells were mostly spherical in the case of the Mg blowing agent whereas AlMg50 and AlMg40 blowing agents produced polyhedral cells. The foams produced by using AlMg50 powders have the

Table VI. Cell Wall Length, Cell Wall Thickness and Aspect Ratio of Foams Produced Using Different Blowing Agents

Blowing Agent	Cell Wall Length, L (mm)	Cell Wall Thickness, $t_{1/2}$ (mm)	Aspect Ratio, $t_{1/2}/L$
Mg	0.95	0.071	0.08
AlMg50-MM-15 min	0.69	0.087	0.13
AlMg40-MM-5 min	0.34	0.075	0.25

highest strength. However, when considering defect-free structures, foam produced using AlMg40 powders showed the highest compressive strength due to its small cells with thicker cell walls.

Compared to AlMg50 and AlMg40 powders, the production of Mg powders is more challenging because of a high tendency of oxidation during the melting of Mg. Consequently, the cost of Mg powders is expected to be much higher than that of AlMg50 and AlMg40 powders. Therefore, although all the blowing agents resulted in foams with good structure and high strength, AlMg50 and AlMg40 blowing agents should be preferred for commercial productions of aluminum foams.

ACKNOWLEDGMENT

The authors thank the Naval Research Board of Defence Research and Development Organization, India, for funding this study through project number NRB-371/MAT/15-16.

CONFLICT OF INTEREST

The authors declare that they have no known competing financial interests or personal relationships that could have appeared to influence the work reported in this paper.

ELECTRONIC SUPPLEMENTARY MATERIAL

The online version of this article (https://doi.org/10.1007/s11663-020-02008-2) contains supplementary material, which is available to authorized users.

REFERENCES

1. J. Banhart: *Progress Mater. Sci.*, 2001, vol. 46, pp. 559–632.
2. F. García-Moreno: *Materials*, 2016, vol. 9, pp. 85–111.
3. J. Banhart and H.W. Seeliger: *Adv. Eng. Mater.*, 2008, vol. 10, pp. 793–802.
4. L.J. Gibson and M.F. Ashby: *Cellular Solids: Structure and Properties*, Cambridge University Press, Cambridge, 1999.
5. S. Kim and C.-W. Lee: *Procedia Mater. Sci.*, 2014, vol. 4, pp. 305–09.
6. M. Mukherjee, U. Ramamurty, F. Garcia-Moreno, and J. Banhart: *Acta Mater.*, 2010, vol. 58, pp. 5031–42.
7. B. Matijasevic-Lux, J. Banhart, S. Fiechter, O. Görke, and N. Wanderka: *Acta Mater.*, 2006, vol. 54, pp. 1887–900.
8. P.H. Kamm, F. García-Moreno, C. Jiménez, and J. Banhart: *J. Mater. Res.*, 2013, vol. 28, pp. 2436–43.
9. T. Koizumi, K. Kido, K. Kita, K. Mikado, S. Gnyloskurenko, and T. Nakamura: *Mater. Trans.*, 2011, vol. 52, pp. 728–33.
10. B. Matijasevic, O. Görke, H. Schubert and J. Banhart: *Proceedings of JIMIC-4 MetFoam2005, Porous Metals and Metal Foaming Technology*. 2006.
11. C. Jiménez, F. Garcia-Moreno, B. Pfretzschner, M. Klaus, M. Wollgarten, I. Zizak, G. Schumacher, M. Tovar, and J. Banhart: *Acta Mater.*, 2011, vol. 59, pp. 6318–30.
12. L. Helfen, T. Baumbach, H. Stanzick, J. Banhart, A. Elmoutaouakkil, and P. Cloetens: *Adv. Eng. Mater.*, 2002, vol. 4, pp. 808–13.
13. M. Mukherjee, F. Garcia-Moreno, and J. Banhart: *Scripta Mater.*, 2010, vol. 63, pp. 235–38.
14. A. Andreasen: *Int. J. Hydrogen Energy*, 2008, vol. 33, pp. 7489–97.
15. C. Jiménez, F. Garcia-Moreno, J. Banhart, G. Zehl, L.P. Lefebvre, and D. Dunand: *Porous Metals Metal. Foams Metfoam*, 2008, vol. 2007, pp. 59–62.
16. M. Mukherjee, F. Garcia-Moreno, C. Jiménez, and J. Banhart: *Adv. Eng. Mater.*, 2010, vol. 12, pp. 472–77.
17. S. Bouaricha, J.P. Dodelet, D. Guay, J. Huot, S. Boily, and R. Schulz: *J. Alloys Compd.*, 2000, vol. 297, pp. 282–93.
18. E.W. Andrews, G. Gioux, P. Onck, and L.J. Gibson: *Int. J. Mech. Sci.*, 2001, vol. 43, pp. 701–13.
19. I. Jeon and T. Asahina: *Acta Mater.*, 2005, vol. 53, pp. 3415–23.
20. H. Okamoto: *J. Phase Equilib. Diffus.*, 1998, vol. 19, p. 598.
21. A.K. Chaubey, S. Scudino, M. Samadi Khoshkhoo, K.G. Prashanth, N.K. Mukhopadhyay, B.K. Mishra, and J. Eckert: *J. Alloys Compd.*, 2014, vol. 610, pp. 456–61.
22. A.R. Cooper, Jr and L.E. Eaton: *J. Am. Ceram. Soc.*, 1962, vol. 45, pp. 97–101.
23. C. Suryanarayana: *Prog. Mater Sci.*, 2001, vol. 46, pp. 1–184.
24. K.A. Nazari, A. Nouri, and T. Hilditch: *Mater. Lett.*, 2015, vol. 140, pp. 55–58.
25. A. Azimi, A. Shokuhfar, and A. Zolriasatein: *Mater. Sci. Eng. A*, 2014, vol. 595, pp. 124–30.
26. J. Baumeister and H. Schrader: *U.S. Patent 5151246 A*, 1992.
27. C. Jiménez, F. Garcia-Moreno, M. Mukherjee, O. Goerke, and J. Banhart: *Scripta Mater.*, 2009, vol. 61, pp. 552–55.
28. J. Karch, R. Birringer, and H. Gleiter: *Nature*, 1987, vol. 330, pp. 556–558.
29. M.J. Mayo, R.W. Siegel, Y.X. Liao, and W.D. Nix: *J. Mater. Res.*, 1992, vol. 7, pp. 973–79.
30. R.N. Lumley, T.B. Sercombe, and G.M. Schaffer: *Metall. Mater. Trans. A*, 1999, vol. 30A, pp. 457–63.
31. K. Kondoh, A. Kimura, and R. Watanabe: *Powder Metall.*, 2001, vol. 44, pp. 161–64.
32. A. Andreasen: Report No. 8755034594, *Risø National Laboratory, Denmark*, 2005.
33. C. Körner, M. Thies, and R.F. Singer: *Adv. Eng. Mater.*, 2002, vol. 4, pp. 765–69.
34. B. Vigeholm, K. Jensen, B. Larsen, and A. Schrøder Pedersen: *J. Less Common Met.*, 1987, vol. 131, pp. 133–41.
35. P. Selvam, B. Viswanathan, C.S. Swamy, and V. Srinivasan: *Int. J. Hydrogen Energy*, 1986, vol. 11, pp. 169–92.
36. P.S. Rudman: *J. Appl. Phys.*, 1979, vol. 50, pp. 7195–99.
37. W.E. Wallace, R.S. Craig, and V.U.S. Rao: *Department of Chemistry, University of Pittsburgh*, 1978.
38. L. Schlapbach, A. Seiler, and F. Stucki: *Mater. Res. Bull.*, 1979, vol. 14, pp. 785–90.
39. L. Helfen, T. Baumbach, P. Pernot, P. Cloetens, H. Stanzick, K. Schladitz, and J. Banhart: *Appl. Phys. Lett.*, 2005, vol. 86, p. 231907.
40. A. Rack, H.-M. Helwig, A. Bütow, A. Rueda, B. Matijašević-Lux, L. Helfen, J. Goebbels, and J. Banhart: *Acta Mater.*, 2009, vol. 57, pp. 4809–21.

41. D.L. Weaire and S. Hutzler: *The Physics of Foams*, Oxford University Press, Oxford, 2001.
42. L.J. Gibson: *Annu. Rev. Mater. Sci.*, 2000, vol. 30, pp. 191–227.
43. M. Kolluri, M. Mukherjee, F. Garcia-Moreno, J. Banhart, and U. Ramamurty: *Acta Mater.*, 2008, vol. 56, pp. 1114–25.
44. Y. Sugimura, A. Rabiei, A.G. Evans, A.M. Harte, and N.A. Fleck: *Mater. Sci. Eng. A*, 1999, vol. 269, pp. 38–48.
45. T. Miyoshi, M. Itoh, T. Mukai, H. Kanahashi, H. Kohzu, S. Tanabe, and K. Higashi: *Scripta Mater.*, 1999, vol. 41, pp. 1055–60.
46. L.J. Gibson, M.F. Ashby, J. Zhang, and T.C. Triantafillou: *Int. J. Mech. Sci.*, 1989, vol. 31, pp. 635–63.
47. S. Lee, F. Barthelat, N. Moldovan, H.D. Espinosa, and H.N.G. Wadley: *Int. J. Solids Struct.*, 2006, vol. 43, pp. 53–73.
48. C.E. Wen, Y. Yamada, K. Shimojima, Y. Chino, H. Hosokawa, and M. Mabuchi: *Mater. Lett.*, 2004, vol. 58, pp. 357–60.